

Article

# A New Family of Heterometallic $\text{Ln}^{\text{III}}[12\text{-MC}_{\text{Fe}^{\text{III}}\text{N}(\text{shi})\text{-4}]$ Complexes: Syntheses, Structures and Magnetic Properties

Tingting Lou, Hua Yang, Suyuan Zeng, Dacheng Li and Jianmin Dou \*

Shandong Provincial Key Laboratory of Chemical Energy Storage and Novel Cell Technology, School of Chemistry and Chemical Engineering, Liaocheng University, Liaocheng 252059, China; loucunjie@163.com (T.L.); yanghua\_1101@163.com (H.Y.); drzengsy@163.com (S.Z.); lidacheng62@163.com (D.L.)

\* Correspondence: dougroup@163.com; Tel.: +86-0635-8239298

Received: 21 April 2018; Accepted: 17 May 2018; Published: 19 May 2018



**Abstract:** A new family of  $\text{Ln}^{\text{III}}$  [12-Metallacrown-4] compounds of formulas  $(\text{C}_5\text{H}_6\text{N})[\text{LnFe}_4(\text{shi})_4(\text{C}_6\text{H}_5\text{COO})_4(\text{Py})_4]\cdot 3.5\text{Py}$  [ $\text{Ln} = \text{Eu}^{\text{III}}$  (1);  $\text{Gd}^{\text{III}}$  (2);  $\text{Tb}^{\text{III}}$  (3);  $\text{Dy}^{\text{III}}$  (4); and,  $\text{H}_3\text{shi} = \text{salicylhydroxamic acid}$ ] were obtained through one-pot reactions with  $\text{H}_3\text{shi}$ ,  $\text{Fe}(\text{NO}_3)_3\cdot 9\text{H}_2\text{O}$ , and,  $\text{Ln}(\text{NO}_3)_3\cdot 6\text{H}_2\text{O}$  as reagents. Single-crystal X-ray analyses show that they are isostructural and have the similar  $[12\text{-MC}_{\text{Fe}^{\text{III}}\text{N}(\text{shi})\text{-4}]$  core, with four benzoate molecules bridging the central  $\text{Ln}^{\text{III}}$  ion to the ring  $\text{Fe}^{\text{III}}$  ions. The negative charge of the 12-MC-4 metallacrown is balanced by one pyridinium cation, which forms the hydrogen bond with an adjacent solvent pyridine molecule. Magnetic measurements demonstrate antiferromagnetic coupling interactions and field-induced slow magnetic relaxation in complex 4.

**Keywords:** salicylhydroxamic acid; metallacrown; crystal structure; 3d-4f; slow magnetic relaxation

## 1. Introduction

With the rapid development of information technology, it is essential to produce information storage materials with higher storage density and faster response speed. Single molecule magnet (SMM), acting as a separate magnetic domain, behaves potential applications in information storage and quantum computation [1–4]. The first SMM was reported in 1993 [5], then, such cases have attracted considerable attention from chemists and physicists due to their unique magnetic properties [6–9]. As we all know, the involved metallic ions for the studies of SMMs mainly consist of paramagnetic three-dimensional (3d) ions, heterometallic 3d-4f ions and homometallic 4f ions. With the high magnetic anisotropy of 3d ions and large spin-orbital coupling of 4f ions, the heterometallic 3d-4f complexes have represented extreme properties in magnetic investigations. So far, the most studied 3d-4f complexes include heterometallic Mn-Ln, Cu-Ln [10,11], Zn-Ln [12], and Co-Ln [13,14], SMMs, and a few Fe-Ln SMMs. Furthermore, the survey of heterometallic Fe-Ln complexes only shows  $\text{Fe}_2\text{Ln}_2$  and  $\text{Fe}_3\text{LnO}_2$  butterfly core [15,16],  $\text{Fe}_2\text{Ln}$  triangular system [17], and  $\text{Fe}_4\text{Dy}_2$  S-shape [18] structural frameworks. Few cyclic Fe-Ln compounds have been documented [19,20]. Therefore, it is interesting to investigate the heterometallic Fe-Ln complexes with cyclic structures and to explore their magnetic properties.

Metallacrowns (MCs), which are a type of metallic macrocyclic polynuclear complexes, are usually regarded as metal ions and nitrogen atoms instead of methylene carbons of organic crowns [21,22]. The first MC with the formula represented by  $\{[\text{VO}(\text{shi})(\text{MeOH})]_3(9\text{-MC-3})\}$  shi = salicylhydroxamic acid} was reported in 1989 [23], since then, a great deal of metallacrowns with different structural types from 9-MC-3 to 60-MC-20 have been explored [24–28]. The ring metal ions for these MCs contain

homogeneous 3d ions or heterometallic 3d-4f ions. For 3d-4f MCs, they embody Mn-Ln<sup>III</sup> [12-MC-4], Mn-Ln<sup>III</sup> [14-MC-5], and Cu-Ln<sup>III</sup> [15-MC-5] structural types [29,30]. Recently, a series of Zn-Ln MCs also have been documented with two [12-MC<sub>Zn</sub>-4] MC units capping a Ln<sup>III</sup> [24-MC<sub>Zn</sub>-8] unit to form a sandwich motif and possess near-infrared luminescent [31]. Nevertheless, few MCs consisting of Fe-Ln ions have been found, except that several homometallic [9-MC<sub>Fe</sub><sup>III</sup>-3], [18-MC<sub>Fe</sub><sup>III</sup>-6] MCs, and a family of 18-MC-6 azametallacrowns have exhibited charming structures and magnetic properties [24,32–34]. Due to the high magnetic anisotropy and large spin-orbital coupling of Ln<sup>III</sup> ions, as well as high-spin Fe<sup>III</sup> with  $S = 5/2$  spin state presenting Spin Crossover (SCO) [35–38], it is meaningful to explore macrocyclic polynuclear complexes with Fe-Ln MCs structures and magnetic properties.

In the previous research, only a family of Fe<sup>III</sup>-Ln [18-MC-6] MCs [34] have been published. In order to further expand Fe-Ln MCs structural types and to study their magnetic properties, we synthesized a series of new Ln<sup>III</sup> [12-MC<sub>Fe</sub><sup>III</sup><sub>N(shi)</sub>-4] [Ln = Eu<sup>III</sup> (1), Gd<sup>III</sup> (2), Tb<sup>III</sup> (3), Dy<sup>III</sup> (4)] complexes through the reactions of salicylhydroxamic acid (H<sub>3</sub>shi) and the corresponding metal salts. Their structures were characterized by X-ray single diffraction and the magnetic properties were also explored in detail.

## 2. Materials and Methods

### 2.1. Materials

Salicylhydroxamic acid, Fe(NO<sub>3</sub>)<sub>3</sub>·9H<sub>2</sub>O, Ln(NO<sub>3</sub>)<sub>3</sub>·6H<sub>2</sub>O, sodium benzoate, CH<sub>3</sub>OH, and pyridine. All of the reagents were commercially available without further purification.

### 2.2. Physical Methods

Elemental analyses for carbon, hydrogen, and nitrogen were tested by Elementar Vario EL analyzer (Elementar, Langensfeld, Germany). The IR spectra were measured on a Perkin-Elmer Spectrum (Thermo Nicolet Corporation, Madison, WI, USA) with samples being prepared as KBr pellets. The XRD patterns were recorded using a XD-3 system with a CuKα radiation (General Analysis Corporation, Beijing, China) source ( $\lambda = 1.54 \text{ \AA}$ ) at 36 keV and 20 mA in the  $2\theta$  range between 5° and 50°, at 0.04 steps every 4 s. Magnetic measurements on crystalline samples were carried out in the temperature range of 1.8–300 K under an applied field of 1000 Oe by using a Quantum Design MPMS-XL7 SQUID magnetometer (Quantum Design, San Diego, CA, USA). AC susceptibilities were investigated in a zero-applied dc field and 2000 Oe dc field for 1–3 and 1000 Oe dc field for 4, with oscillating frequencies of 1–999 Hz.

### 2.3. Syntheses

#### 2.3.1. (C<sub>5</sub>H<sub>6</sub>N)[EuFe<sub>4</sub>(shi)<sub>4</sub>(C<sub>6</sub>H<sub>5</sub>COO)<sub>4</sub>(Py)<sub>4</sub>].3.5Py (1)

Salicylhydroxamic acid (H<sub>3</sub>shi) (0.2 mmol), Fe(NO<sub>3</sub>)<sub>3</sub>·9H<sub>2</sub>O (0.2 mmol), Eu(NO<sub>3</sub>)<sub>3</sub>·6H<sub>2</sub>O (0.05 mmol), and sodium benzoate (0.6 mmol) were dissolved in a mixed solution of 20 mL MeOH and 2 mL pyridine, resulting in a clear, black-red solution and then stirred for six hours. The solution was then filtered and the filtrate was placed in a dark cupboard for crystal growth. The black-red single crystals were yielded after 12 days through the slow evaporation of the black-red solution. The yield was 35.0 mg (32.8%, based on Eu). Elemental analysis (%) calcd for C<sub>98.5</sub>H<sub>79.5</sub>Fe<sub>4</sub>EuN<sub>12.5</sub>O<sub>20</sub>: C, 55.45; H, 3.76; N, 8.21. Found: C, 55.06; H, 3.36; N, 8.58. IR (KBr), cm<sup>-1</sup>: 3456 [ $\nu$ (O-H)], 1597 [ $\nu$ (C=N)<sub>shi</sub>], 1564 [ $\nu$ (C=O)<sub>benzoate</sub>], 1446 [ $\nu$ (C=O)<sub>benzoate</sub>], and 1262 [ $\nu$ (N-O<sub>ox</sub>)<sub>shi</sub>]. The purity of the single-crystal samples was determined by the powder X-ray diffraction analyses (Figure S1).

#### 2.3.2. (C<sub>5</sub>H<sub>6</sub>N)[GdFe<sub>4</sub>(shi)<sub>4</sub>(C<sub>6</sub>H<sub>5</sub>COO)<sub>4</sub>(Py)<sub>4</sub>].3.5Py (2)

The complex 2 was obtained by the same way for 1 with Gd(NO<sub>3</sub>)<sub>3</sub>·6H<sub>2</sub>O (0.05 mmol) instead of Eu(NO<sub>3</sub>)<sub>3</sub>·6H<sub>2</sub>O. The black-red single crystals were yielded after 10 days through the slow evaporation

of the black-red solution. The yield was 37.8 mg (35.4%, based on Gd). Elemental analysis (%) calcd for  $C_{98.5}H_{79.5}Fe_4GdN_{12.5}O_{20}$ : C, 55.31; H, 3.75; N, 8.19. Found: C, 55.04; H, 3.35; N, 8.52. IR (KBr),  $cm^{-1}$ : 3460 [ $\nu(O-H)$ ], 1597 [ $\nu(C=N)_{shi}$ ], 1563 [ $asym(CO_2)_{benzoate}$ ], 1446 [ $sym(CO_2)_{benzoate}$ ], and 1262 [ $(N-O_{ox})_{shi}$ ]. The purity of the single-crystal samples was determined by the powder X-ray diffraction analyses (Figure S1).

### 2.3.3. $(C_5H_6N)[TbFe_4(shi)_4(C_6H_5COO)_4(Py)_4] \cdot 3.5Py$ (3)

The complex **3** was obtained by the same way for **1** with  $Tb(NO_3)_3 \cdot 6H_2O$  (0.05 mmol) instead of  $Eu(NO_3)_3 \cdot 6H_2O$ . The black-red single crystals were yielded after 13 days through the slow evaporation of the black-red solution. The yield was 45.4 mg (42.4%, based on Tb). Elemental analysis (%) calcd for  $C_{98.5}H_{79.5}Fe_4TbN_{12.5}O_{20}$ : C, 55.27; H, 3.74; N, 8.18. Found: C, 55.63; H, 3.43; N, 8.45. IR (KBr),  $cm^{-1}$ : 3448 [ $\nu(O-H)$ ], 1597 [ $\nu(C=N)_{shi}$ ], 1564 [ $asym(CO_2)_{benzoate}$ ], 1447 [ $sym(CO_2)_{benzoate}$ ], and 1262 [ $(N-O_{ox})_{shi}$ ]. The purity of the single-crystal samples was determined by the powder X-ray diffraction analyses (Figure S1).

### 2.3.4. $(C_5H_6N)[DyFe_4(shi)_4(C_6H_5COO)_4(Py)_4] \cdot 3.5Py$ (4)

The complex **2** was obtained by the same way for **1** with  $Dy(NO_3)_3 \cdot 6H_2O$  (0.05 mmol) instead of  $Eu(NO_3)_3 \cdot 6H_2O$ . The black-red single crystals were yielded after 15 days through the slow evaporation of the black-red solution. The yield was 40.3 mg (37.6%, based on Dy). Elemental analysis (%) calcd for  $C_{98.5}H_{79.5}Fe_4DyN_{12.5}O_{20}$ : C, 55.18; H, 3.74; N, 8.17. Found: C, 55.56; H, 3.42; N, 8.52. IR (KBr),  $cm^{-1}$ : 3456 [ $\nu(O-H)$ ], 1597 [ $\nu(C=N)_{shi}$ ], 1564 [ $asym(CO_2)_{benzoate}$ ], 1446 [ $sym(CO_2)_{benzoate}$ ], and 1262 [ $(N-O_{ox})_{shi}$ ]. The purity of the single-crystal samples was determined by the powder X-ray diffraction analyses (Figure S1).

## 2.4. X-ray Crystallography

Single-crystal X-ray diffraction data for compounds **1–4** were collected on a Bruker Smart CCD area-detector diffractometer (Bruker AXS Inc., Madison, WI, USA,  $MoK\alpha$ ,  $\lambda = 0.71073 \text{ \AA}$ ) by  $\omega$ -scan mode operating at 298 K. The program SAINT (version 2014/7) was used for the integration of the diffraction profiles and semiempirical absorption corrections were applied using SADABS (version 2.03). All of the structures were solved by direct methods using the SHELXS (version 2014/7) program of the SHELXTL (version 2014/7) package, and were refined by full-matrix least-squares methods with SHELXL [39]. Further details for crystallography are listed in Table 1.

**Table 1.** Crystal data and structure refinement for complexes **1–4**.

	<b>1</b>	<b>2</b>	<b>3</b>	<b>4</b>
Empirical formula	$C_{98.5}H_{79.5}Fe_4N_{12.5}O_{20}Eu$	$C_{98.5}H_{79.5}Fe_4N_{12.5}O_{20}Gd$	$C_{98.5}H_{79.5}Fe_4N_{12.5}O_{20}Tb$	$C_{98.5}H_{79.5}Fe_4N_{12.5}O_{20}Dy$
Formula weight	2133.60	2138.89	2140.57	2144.15
T(K)	298(2)	298(2)	298(2)	298(2)
Crystal system	Monoclinic	Monoclinic	Monoclinic	Monoclinic
Space group	P2(1)/n	P2(1)/n	P2(1)/n	P2(1)/n
$a(\text{\AA})$	14.3022(13)	14.2222(13)	14.2903(13)	14.3011(13)
$b(\text{\AA})$	34.152(3)	33.248(3)	34.258(3)	34.231(3)
$c(\text{\AA})$	19.4743(17)	19.3213(17)	19.4615(16)	19.5141(17)
$\alpha(^{\circ})$	90	90	90	90
$\beta(^{\circ})$	106.772(2)	105.913(3)	106.756(3)	106.873(3)
$\gamma(^{\circ})$	90	90	90	90
$V(\text{\AA}^3)$	9107.6(14)	8786.0(13)	9123.1(14)	9141.7(14)
Z	4	4	4	4

Table 1. Cont.

	1	2	3	4
$D_c$ (Mg·m <sup>-3</sup> )	1.556	1.617	1.558	1.558
$\mu$ (mm <sup>-1</sup> )	1.381	1.472	1.466	1.507
Data/parameters	16,024/10,074	15,469/10,476	16,064/10,256	16,090/10,256
$R_{\text{int}}$	0.0647	0.0664	0.0675	0.0724
GOOF ( $F^2$ )	1.020	1.082	1.067	1.047
$R_1$ [ $I > 2\sigma(I)$ ]	0.0594	0.0681	0.0677	0.0706
$wR_2$ (all data)	0.1046	0.1514	0.1513	0.1846

CCDC 1582199, 1582197, 1582195 and 1582194 contain the supplementary crystallographic data for 1–4. These data can be obtained free of charge via <http://www.ccdc.cam.ac.uk/conts/retrieving.html>, or from the Cambridge Crystallographic Data Centre, 12 Union Road, Cambridge CB2 1EZ, UK; fax: +44-1223-336-033; or e-mail: deposit@ccdc.cam.ac.uk.

### 3. Results and Discussion

#### 3.1. Description of Crystal Structures

Single-crystal X-ray structural analyses indicate that 1–4 are isostructural heterometallic compounds. The molecular structure of complexes 1–4 are shown in Figure 1a–d. The complex 4 is described as a representative example in detail. It crystallizes in the monoclinic space group  $P2_1/n$ . The asymmetrical unit includes a representative 12-MC<sub>Fe<sup>III</sup></sub><sup>shi</sup>-4 structural framework, which is composed of four Fe<sup>III</sup> ions, four deprotonated shi<sup>3-</sup> ligands, four benzoate ligands, four dative pyridine molecules, and one Dy<sup>III</sup> ion. The oxidation states of four Fe ions were determined through the bond lengths, charge balance, and the BVS calculations with the values, as shown in Table S1. The Fe 2p XP spectra of a monolayer of complexes 1–4 further prove the the oxydation state of Fe ions [40] (Figure S3, Table S5). Each Fe<sup>III</sup> ion is six-coordinated with N<sub>2</sub>O<sub>4</sub> atoms from carbonyl oxygen, oxime oxygen, hydroxyl oxygen, oxime nitrogen, pyridyl nitrogen, and benzoate oxygen, respectively. Further, each fully deprotonated shi<sup>3-</sup> ligand links two adjacent Fe<sup>III</sup> ions through their oxime oxygen and oxime nitrogen to form the N–O bridgings between these Fe<sup>III</sup> ions. Thus, four Fe<sup>III</sup> ions and four shi<sup>3-</sup> ligands are held together to form a 12-MC-4 MC core with the ring presenting Fe–N–O repeat unit. For these four shi<sup>3-</sup> ligands, an obvious difference is that three ligands are located in the MC plane, and the fourth ligand is nearly perpendicular to the MC plane. It may be attributed to the steric hindrance to make the fourth ligand distortion. The dihedral angle between the twisted ligand and the MC plane is 81.8(9)°.

Interestingly, one Dy<sup>III</sup> ion that is encapsulated in the cavity of 12-MC-4 ring. Dy<sup>III</sup> ion is located in eight coordination environment with the coordination atoms from MC ring four oxygen atoms and four <sup>-</sup>Obz carbonyl oxygen atoms (Figure S2a). For the coordination configuration of Dy<sup>III</sup> ions, the parameter  $\alpha$  is usually used to depict the elongation or the flatness in a square antiprism.  $\alpha$  is calculated through the S<sub>8</sub> axis of the square antiprism, and the central atom ligand bond, in the meantime, it is also can be defined as  $\gamma/2$ , where  $\gamma$  is the angle between opposite ligands within one hemisphere. For complex 4, the values of  $\gamma$  angles for Dy1 are 119.701(195)° (O14–Dy1–O11), 117.036(199)° (O16–Dy1–O13), 108.037(189)° (O5–Dy1–O20), and 111.726(196)° (O3–Dy1–O8), respectively. The  $\alpha$  angles of 59.851° (O14, O11) and 58.518° (O16, O13) in the hemisphere (O14, O13, O11, and O16), as well as 54.019° (O5, O20) and 55.863° (O3, O8) in the hemisphere (O8, O5, O3, and O20) are slightly deviated from the theoretical value (57.16°) by 2.691, 1.358, 3.141, and 1.297°, respectively. Complexes 1–3 also possess eight-coordination with a distorted square antiprism geometry (Figure S2b–d), and the angles are shown in Table S2. The encapsulated Dy<sup>III</sup> ion and ring Fe<sup>III</sup> ions are further bridged through two oxygen atoms of <sup>-</sup>Obz groups with the bond lengths of Fe–O and Dy–O in the ranges 2.361(6)–2.475(5) and 1.901(6)–2.041(6) Å, and the angles of Fe–O–Dy in the range 119.2(2)–123.2(2)°, respectively.

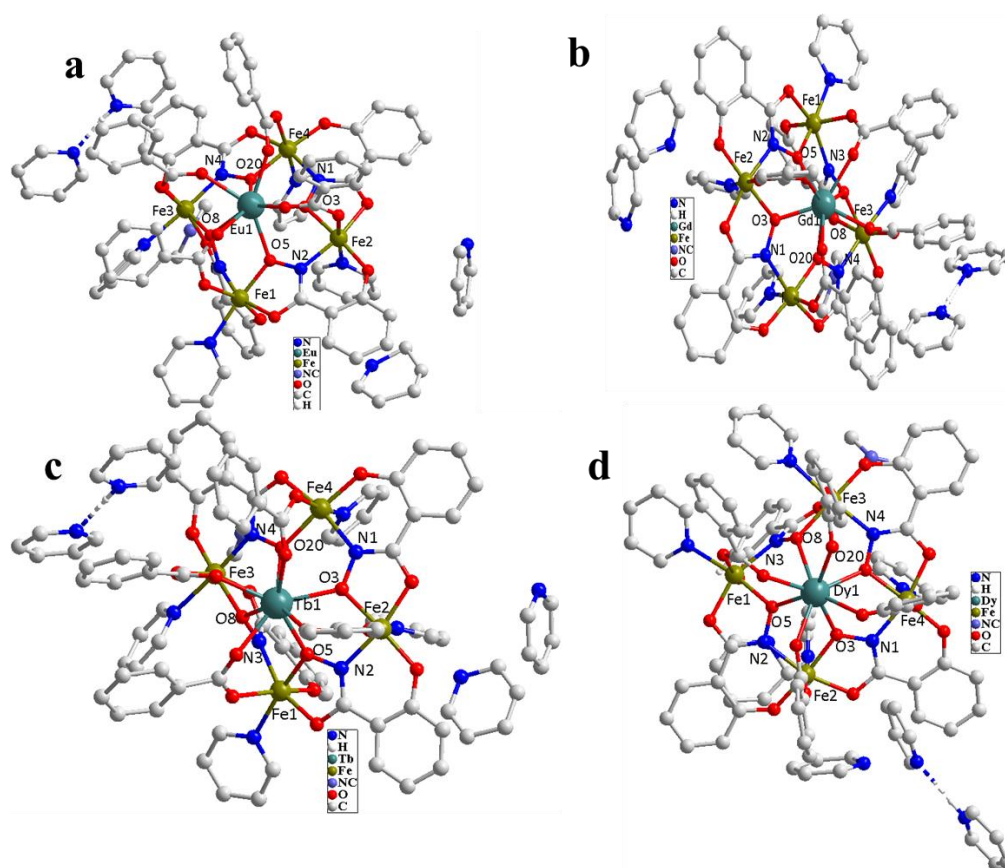


**Figure 1.** Overall molecular structure for complex 1 (a), complex 2 (b), complex 3 (c), and complex 4 (d) (Some hydrogen atoms have been omitted for clarity).

It is worthily noted that the 12-MC-4 MC unit displays the negative valence with its charge balanced by one pyridinium cation, where the pyridine nitrogen is protonated. The angle of C–N–C is  $138.748(254)^\circ$ , which is larger than that of the parent pyridine complex, which results in the occurrence of the protonation on this site [41–43]. Meanwhile, the hydrogen bond interaction is formed between the pyridinium cation and an adjacent pyridine molecule, which is also reported in [12-MC<sub>Ga</sub><sup>III</sup><sub>N(shi)</sub>-4] [44].

Complexes 1–3 have the similar structural configuration with 4 and the difference is discussed. The deviation distances of Ln<sup>III</sup> ions to the oxime oxygen mean plane (O<sub>ox</sub>MP) and to the Fe<sup>III</sup> mean plane (FeMP) are shown in Table 2. From the data, we can see that, as the radius of Ln<sup>III</sup> ions decrease, the Ln<sup>III</sup> are approach the plane much more. The similar tendency was also observed in the reported 12-MC<sub>Mn</sub><sup>III</sup><sub>(N)shi</sub>-4 [45]. The distances between Ln–O and the distortion angles of benzoate for these four complexes are slightly different, further details are shown in Tables S3 and S4.

**Table 2.** The deviation distance from Ln<sup>III</sup> ions to O<sub>ox</sub>MP and FeMP.

Compound	Ln <sup>III</sup> -O <sub>ox</sub> MP distance (Å)	Ln <sup>III</sup> -FeMP distance (Å)
Fe <sub>4</sub> Eu (1)	1.3943 (3)	1.7826 (3)
Fe <sub>4</sub> Gd (2)	1.3875 (4)	1.7728 (4)
Fe <sub>4</sub> Tb (3)	1.3867 (4)	1.7589 (4)
Fe <sub>4</sub> Dy (4)	1.3864 (4)	1.7505 (4)

### 3.2. Magnetic Properties

The variable temperature magnetic susceptibilities of the complexes 1–4 were determined in the temperature range of 1.8–300 K and an applied field of 0.1 T. The  $\chi_M T$  versus  $T$  plots are shown in Figure 2. The values of  $\chi_M T$  for complexes 1–4 are 16.20 (1), 21.27 (2), 26.01 (3), and 29.22 (4)  $\text{cm}^3 \text{mol}^{-1} \text{K}$  at 300 K, respectively, which are lower than expected values of non-interacting four  $\text{Fe}^{\text{III}}$  ions ( $d^5$ ,  $S = 5/2$ ,  $g = 2$ ) and one  $\text{Ln}^{\text{III}}$  [ $\text{Eu}^{\text{III}}$ ,  ${}^7F_0$ ;  $\text{Gd}^{\text{III}}$ ,  ${}^8S_{7/2}$ ,  $g = 2$ ;  $\text{Tb}^{\text{III}}$ ,  ${}^7F_6$ ,  $g = 3/2$ ;  $\text{Dy}^{\text{III}}$ ,  ${}^6H_{15/2}$ ,  $g = 4/3$ ] ion of 19.00 (1), 25.21 (2), 29.15 (3), and 31.50 (4)  $\text{cm}^3 \text{mol}^{-1} \text{K}$ . With the temperature reducing, the  $\chi_M T$  values decrease gradually to 0.18 (1), 7.90 (2), 8.62 (3), and 11.01 (4)  $\text{cm}^3 \text{mol}^{-1} \text{K}$  at 1.8 K, respectively (Table 3), manifesting the antiferromagnetic coupling in the complexes. The fitting of the Curie-Weiss law for the high-temperature  $\chi_M T$  values resulted in different  $\theta$  values, with  $-131.96$  K,  $-59.83$  K,  $-43.72$  K, and  $-40.00$  K for complexes 1–4, respectively.

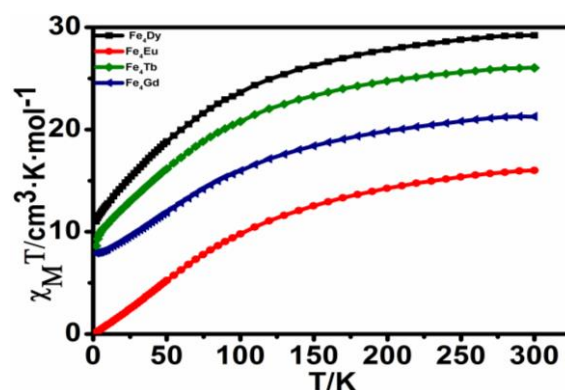


Figure 2.  $\chi_M T$  vs.  $T$  plots for complexes 1–4 in an applied 1000 Oe dc field.

Table 3. Expected and measured  $\chi_M T$  values for 1–4.

Compound	Expected spin only value ( $\text{cm}^3 \text{mol}^{-1} \text{K}$ )	Measured value at 300 K ( $\text{cm}^3 \text{mol}^{-1} \text{K}$ )	Measured value at 1.8 K ( $\text{cm}^3 \text{mol}^{-1} \text{K}$ )
$\text{Fe}_4\text{Eu}$ (1)	19	16.2	0.18
$\text{Fe}_4\text{Gd}$ (2)	25.21	21.27	7.9
$\text{Fe}_4\text{Tb}$ (3)	29.15	26.01	8.62
$\text{Fe}_4\text{Dy}$ (4)	31.5	29.22	11.01

Similar to other reported Fe-Ln complexes, the magnetic behavior of this series of compounds is also related to the  $\text{Fe}^{\text{III}}\text{-Fe}^{\text{III}}$ ,  $\text{Fe}^{\text{III}}\text{-Ln}^{\text{III}}$ , and the intrinsic magnetic properties of the  $\text{Ln}^{\text{III}}$  ions. For complex 1, including the  $\text{Eu}^{\text{III}}$  ion, we may try to explore the magnetic interaction mode between metal ions, while for other complexes it is difficult to define. The ground state of  $\text{Eu}^{\text{III}}$  ion is  ${}^7F_0$  and the configuration is  ${}^4f_6$  ( ${}^7F_0$ ,  $S = 3$ ,  $L = 3$ ,  $J = 0$ ). At a low temperature, only the infinitesimal excited states mixing into  ${}^7F_0$  [46] occupied the nonmagnetic ground level. Thus, the magnetic properties of complex 1 at a low temperature are mainly caused by the exchange interaction between  $\text{Fe}^{\text{III}}$  ions. This indicates that the  $\text{Eu}^{\text{III}}$  ion can be deemed to be the diamagnetic ion at low temperature. The extrapolation of  $\chi_M T$  value to 0 K is approaching zero, suggesting that the ground state spin of 1 can be recognized to be  $S = 0$ . Therefore, we can come to a conclusion that the  $\text{Fe}^{\text{III}}\text{-Fe}^{\text{III}}$  interaction mainly lead to the antiferromagnetic behavior of 1. Complexes 2–4 also present antiferromagnetic behavior, but the nonzero ground-state spins may attributed to uncanceled spins between the  $\text{Fe}_4$  unit and  $\text{Ln}^{\text{III}}$  ion. However, owing to the complexity magnetic coupling interactions between  $\text{Fe}^{\text{III}}\text{-Ln}^{\text{III}}$  ( $\text{Gd}^{\text{III}}$ ,  $\text{Tb}^{\text{III}}$ ,  $\text{Dy}^{\text{III}}$ ) and the intrinsic magnetism of  $\text{Ln}^{\text{III}}$  ions, it is very difficult to obtain the appropriate coupling constants for complexes 2–4.

The magnetization of the complexes 1–4 was measured in the 1–7 T magnetic fields and 1.8–8 K temperature range. As shown in Figures S11–S14, the magnetization increases rapidly in the low magnetic field, and then a linear increase without clear saturation at 7 T, with values of  $2.52 \mu_B$  for 1,  $6.42 \mu_B$  for 2,  $5.96 \mu_B$  for 3, and  $6.92 \mu_B$  for 4 at 1.8 K. The reduced magnetization ( $M/N\mu_B - H/T$ ) curves show the non-superposition, suggesting the magnetic anisotropy of metal ions in the molecules and the lack of a well-defined ground state.

In order to further study the magnetic relaxation dynamics of 1–4, the ac susceptibilities were carried out at frequencies in the range of 1–999 Hz and in the temperature range of 1.8–15 K under zero-applied dc field and 2000 Oe dc field for complexes 1–3 and 1000 Oe dc field for complex 4, with a 2.0 Oe ac field oscillating. Complexes 1–4 exhibit similar curves for the in-phase ( $\chi'_M$ ) and out-of-phase ( $\chi''_M$ ) under zero-applied dc field, showing the absence of SMM behavior (Figures S4, S6, S8, and S10). When a 2000 Oe dc field was applied for 1–3 and a 1000 Oe dc field was used for 4, the out-of-phase ( $\chi''_M$ ) signals of complexes 1–3 represent absence of frequency-dependent (Figures S5, S7 and S9), however, complex 4 demonstrates obvious frequency-dependent, revealing the field-induced slow magnetic relaxation (Figure 3). Owing to the absence of maximum value of  $\chi''_M$  for 4, the energy barrier ( $\Delta E_{\text{eff}}$ ) and preexponential factor ( $\tau_0$ ) can only be calculated by the Debye equation:  $\ln(\chi''/\chi') = \ln(\omega\tau_0) + \Delta E_{\text{eff}}/k_B T$  [16,47] (Figure 4). The perfect fitting data are shown in Table 4. The characteristic times is  $10^{-6}$  s for complex 4, values that are in agreement with the observed preexponential factors and effective energy barriers for  $\text{Ln}^{\text{III}}$ -containing SMMs [34]. In our  $\text{Fe}_4\text{Ln}$  analogues, however, only the  $\text{Fe}_4\text{Dy}$  complex represented the magnetic dependence upon the frequencies at 1000 Oe dc field. Maybe the intrinsic properties of trivalent  $\text{Ln}^{\text{III}}$  ions can account for the phenomenon. In most of the coordination environment,  $\text{Dy}^{\text{III}}$ , as the Kramers ion, could always keep the doubly degenerate ground state under the magnetic field. Nevertheless, the non-Kramers ion,  $\text{Tb}^{\text{III}}$ , needs strict axial crystal-field symmetry. Furthermore, the  $\text{Eu}^{\text{III}}$  ion has a ground state of  $J = 0$ , while the  $\text{Gd}^{\text{III}}$  ion is isotropic.

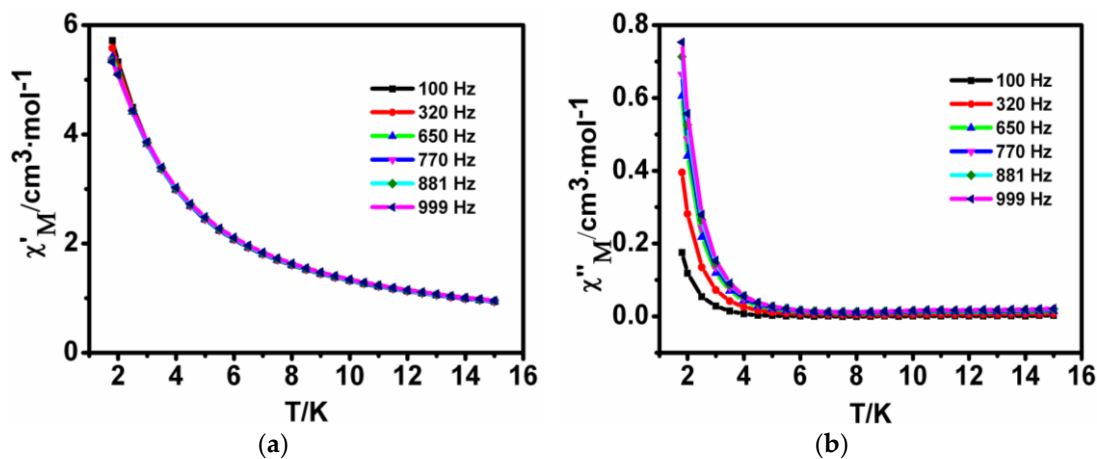


**Figure 3.** (a) Temperature dependence of the in-phase ( $\chi'_M$ ) of ac susceptibility signals for complex 4 measured under a 1000 Oe dc field. (b) Temperature dependence of the out-of phase ( $\chi''_M$ ) of ac susceptibility signals for complex 4 measured under a 1000 Oe dc field.

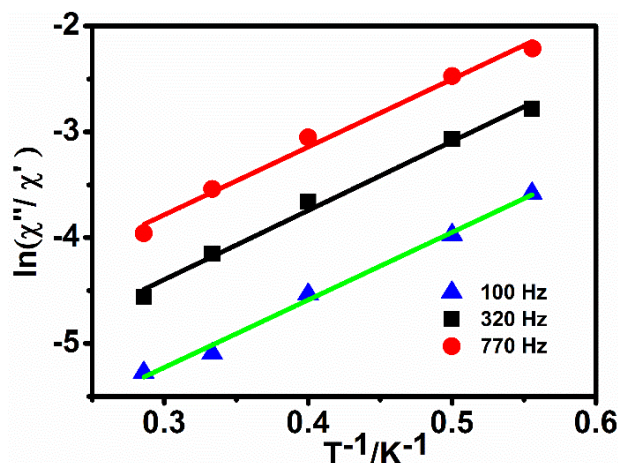


Figure 4. Magnetization relaxation time  $\ln(\chi''/\chi')$  vs  $T^{-1}$  plots for complex 4.

Table 4. Measured  $\Delta E_{\text{eff}}/k_B$  and  $\tau_0$  values for complex 4.

Complex 4		
Frequency (Hz)	$\Delta E_{\text{eff}}/k_B$ (k)	$\tau_0$ (s)
100	4.54	$17.4 \times 10^{-6}$
320	4.49	$9.10 \times 10^{-6}$
770	4.55	$4.64 \times 10^{-6}$

#### 4. Conclusions

We prepared a new family of heterometallic  $\text{Ln}^{\text{III}}$  [12-MC $_{\text{Fe}}^{\text{III}}_{\text{N}(\text{shi})}$ -4] ( $\text{Ln} = \text{Eu}^{\text{III}}, \text{Gd}^{\text{III}}, \text{Tb}^{\text{III}}, \text{Dy}^{\text{III}}$ ) MCs through the one-pot reactions of  $\text{H}_3\text{Shi}$  ligand with the corresponding iron and lanthanide metal salts. The 12-MC-4 structural unit exhibits a monovalent negative ion with the charge being balanced by one pyridinium cation. The arched structure of the 12-MC $_{\text{Fe}}^{\text{III}}_{\text{N}(\text{shi})}$ -4 is related to the radius of  $\text{Ln}^{\text{III}}$  ions, as the  $\text{Ln}^{\text{III}}$  ions' radius decrease, the complex has a less domed structure. The magnetic behavior of the family of compounds was discussed in detail, including the  $\text{Fe}^{\text{III}}\text{-Fe}^{\text{III}}$  and  $\text{Fe}^{\text{III}}\text{-Ln}^{\text{III}}$  interactions.  $\text{Fe}^{\text{III}}\text{-Fe}^{\text{III}}$  interaction within all of the compounds may be antiferromagnetic. The nonzero ground-state spins may attributed to uncanceled spins between the  $\text{Ln}^{\text{III}}$  and  $\text{Fe}^{\text{III}}$  ions. All of the compounds reveal antiferromagnetic behavior and the  $\text{Fe}_4\text{Dy}$  analogue with high anisotropy and large spin shows slow magnetization relaxation at a dc field of 1000 Oe. From the experiment, we can draw a conclusion that the choice of  $\text{Ln}^{\text{III}}$  is important for the SMM properties.

**Supplementary Materials:** The following are available online at <http://www.mdpi.com/2073-4352/8/5/229/s1>, Figure S1: The experimental XRD pattern of samples and the simulated XRD pattern of single crystal X-ray diffraction data for complexes 1–4, Figure S2: Distorted square-antiprismatic geometries around Dy1(a), Eu1(b), Gd1(c), Tb1(d), Figure S3: Fe 2p XP spectras of complexes 1 (a), 2 (b), 3 (c), 4 (d) in monolayers, Figure S4: Temperature dependence of the in-phase ( $\chi''M$ ) and out-of phase ( $\chi''M$ ) ac susceptibility signals of complex 1 measured under 2.0 Oe field with a 0 dc field, Figure S5: Temperature dependence of the in-phase ( $\chi''M$ ) and out-of phase ( $\chi''M$ ) ac susceptibility signals of complex 1 measured under 2.0 Oe field with a 2000 Oe dc field, Figure S6: Temperature dependence of the in-phase ( $\chi''M$ ) and out-of phase ( $\chi''M$ ) ac susceptibility signals of complex 2 measured under 2.0 Oe field with a 0 dc field, Figure S7: Temperature dependence of the in-phase ( $\chi''M$ ) and out-of phase ( $\chi''M$ ) ac susceptibility signals of complex 2 measured under 2.0 Oe field with a 2000 Oe dc field, Figure S8: Temperature dependence of the in-phase ( $\chi''M$ ) and out-of phase ( $\chi''M$ ) ac susceptibility signals of complex 3 measured under 2.0 Oe field with a 0 Oe dc field, Figure S9: Temperature dependence of the in-phase ( $\chi''M$ ) and out-of phase ( $\chi''M$ ) ac susceptibility signals of complex 3 measured under 2.0 Oe field with a 2000 Oe dc field, Figure S10: Temperature dependence of the in-phase ( $\chi''M$ ) and out-of phase ( $\chi''M$ ) ac susceptibility signals of complex 4 measured under 2.0 Oe field with a 0 Oe dc field, Figure S11: Plots of isothermal magnetization  $M$  vs.  $H$  for complex 1 at 1.8–8 K (left). Plots of magnetization  $M$  vs.  $H/T$  for complex 1 at 1–7 T (right), Figure S12: Plots of isothermal magnetization  $M$  vs.  $H$  for complex 2 at 1.8–8 K (left). Plots of magnetization  $M$  vs.  $H/T$  for complex 2 at 1–7 T (right), Figure S13: Plots of isothermal magnetization  $M$  vs.  $H$  for complex 3 at 1.8–8 K (left). Plots of

magnetization M vs. H/T for complex 3 at 1–7 T (right), Figure S14: Plots of isothermal magnetization M vs. H for complex 4 at 1.8–8 K (left). Plots of magnetization M vs. H/T for complex 4 at 1–7 T (right), Table S1: The BVS calculations for complexes 1–4, Table S2: Selected bond angles for complexes 1–3, Table S3: The distances between Ln–O for complexes 1–4, Table S4: The distortion angles of benzoate for complexes 1–4, Table S5: Fit parameters for the Fe 2p XP spectra of complexes 1–4.

**Author Contributions:** T.L., J.D. and D.L. conceived and designed the experiments; T.L. performed the experiments; S.Z. measured properties; T.L. and H.Y. analyzed the data; T.L. wrote the manuscript.

**Funding:** This work was financially supported from the National Natural Science Foundation of China (Grants 21671093 and 21271097).

**Conflicts of Interest:** The authors declare no conflict of interest.

## References

1. Woodruff, D.N.; Winpenny, R.E.P.; Layfield, R.A. Lanthanide Single-Molecule Magnets. *Chem. Rev.* **2016**, *113*, 5110–5148. [[CrossRef](#)] [[PubMed](#)]
2. Liu, K.; Shi, W.; Cheng, P. Toward heterometallic single-molecule magnets: Synthetic strategy, structures and properties of 3d–4f discrete complexes. *Coord. Chem. Rev.* **2015**, *289–290*, 74–122. [[CrossRef](#)]
3. Feltham, H.L.C.; Brooker, S. Review of purely 4f and mixed-metal *nd-4f* single-molecule magnets containing only one lanthanide ion. *Coord. Chem. Rev.* **2014**, *276*, 1–33. [[CrossRef](#)]
4. Gatteschi, D.; Sessoli, R. Quantum Tunneling of Magnetization and Related Phenomena in Molecular Materials. *Angew. Chem. Int. Ed.* **2003**, *42*, 268–297. [[CrossRef](#)] [[PubMed](#)]
5. Sessoli, R.; Gatteschi, D.; Caneschi, A.; Novak, M.A. Magnetic bistability in a metal-ion cluster. *Nature* **1993**, *365*, 141–143. [[CrossRef](#)]
6. Guo, Y.N.; Xu, G.F.; Guo, Y.; Tang, J. Relaxation dynamics of dysprosium(III) single molecule magnets. *Dalton Trans* **2011**, *40*, 9953–9963. [[CrossRef](#)] [[PubMed](#)]
7. Blagg, R.J.; Tuna, F.; McInnes, E.J.L.; Winpenny, R.E.P. Pentametall lanthanide-alkoxide square-based pyramids: High energy barrier for thermal relaxation in a holmium single molecule magnet. *Chem. Commun.* **2011**, *47*, 10587–10589. [[CrossRef](#)] [[PubMed](#)]
8. Chilton, N.F.; Langley, S.K.; Moubaraki, B.; Soncini, A.; Batten, S.R.; Murray, K.S. Single molecule magnetism in a family of mononuclear  $\beta$ -diketonate lanthanide(III) complexes: Rationalization of magnetic anisotropy in complexes of low symmetry. *Chem. Sci.* **2013**, *4*, 1719–1730. [[CrossRef](#)]
9. Zheng, Y.Z.; Zhou, G.J.; Zheng, Z.; Winpenny, R.E.P. Molecule-based magnetic coolers. *Chem. Soc. Rev.* **2014**, *43*, 1462–1475. [[CrossRef](#)] [[PubMed](#)]
10. Xue, S.F.; Guo, Y.N.; Zhao, L.; Zhang, H.X.; Tang, J.K. Molecular Magnetic Investigation of a Family of Octanuclear  $[\text{Cu}_6\text{Ln}_2]$  Nanoclusters. *Inorg. Chem.* **2014**, *53*, 8165–8171. [[CrossRef](#)] [[PubMed](#)]
11. Wu, J.F.; Li, X.L.; Guo, M.; Zhao, L.; Zhang, Y.Q.; Tang, J.K. Realization of toroidal magnetic moments in heterometallic 3d–4f metallocycles. *Chem. Commun.* **2018**, *54*, 1065–1068. [[CrossRef](#)] [[PubMed](#)]
12. Zhang, L.; Zhao, L.; Zhang, P.; Wang, C.; Yuan, S.W.; Tang, J.K. Nanoscale  $\{\text{Ln}^{\text{III}}_{24}\text{Zn}^{\text{II}}_6\}$  Triangular Metalloring with Magnetic Refrigerant, Slow Magnetic Relaxation, and Fluorescent Properties. *Inorg. Chem.* **2015**, *54*, 11535–11541. [[CrossRef](#)] [[PubMed](#)]
13. Wu, J.F.; Zhao, L.; Zhang, L.; Li, X.L.; Guo, M.; Tang, J.K. Metallosupramolecular Coordination Complexes: The Design of Heterometallic 3d–4f Gridlike Structures. *Inorg. Chem.* **2016**, *55*, 5514–5519. [[CrossRef](#)] [[PubMed](#)]
14. Zou, L.F.; Zhao, L.; Guo, Y.N.; Yu, G.M.; Guo, Y.; Tang, J.K.; Li, Y.H. A dodecanuclear heterometallic dysprosium–cobalt wheel exhibiting single-molecule magnet behavior. *Chem. Commun.* **2011**, *47*, 8659–8661. [[CrossRef](#)]
15. Baniodeh, A.; Lan, Y.; Novitchi, G.; Mereacre, V.; Sukhanov, A.; Ferbinteanu, M.; Voronkova, V.; Anson, C.E.; Powell, A.K. Magnetic anisotropy and exchange coupling in a family of isostructural  $\text{Fe}^{\text{III}}_2\text{Ln}^{\text{III}}_2$  complexes. *Dalton Trans.* **2013**, *42*, 8926–8938. [[CrossRef](#)] [[PubMed](#)]
16. Bartolomé, J.; Filoti, G.; Kuncser, V.; Schinteie, G.; Mereacre, V.; Anson, C.E.; Powell, A.K.; Prodius, D.; Turta, C. Magnetostructural correlations in the tetranuclear series of  $\{\text{Fe}_3\text{LnO}_2\}$  butterfly core clusters: Magnetic and Mössbauer spectroscopic study. *Phys. Rev. B: Condens. Matter.* **2009**, *80*, 1–16. [[CrossRef](#)]

17. Singh, N.; Gupta, S.D.; Butcher, R.J.; Christou, G. Synthesis and magnetochemistry of heterometallic triangular  $\text{Fe}^{\text{III}}_2\text{Ln}^{\text{III}}$  (Ln = La, Gd, Tb, Dy, and Ho) and  $\text{Fe}^{\text{III}}_2\text{Y}^{\text{III}}$  complexes. *Dalton Trans.* **2017**, *46*, 7897–7903. [[CrossRef](#)] [[PubMed](#)]
18. Chen, S.; Mereacre, V.; Anson, C.E.; Powell, A.K. A single molecule magnet to single molecule magnet transformation via a solvothermal process:  $\text{Fe}_4\text{Dy}_2 \rightarrow \text{Fe}_6\text{Dy}_3$ . *Dalton Trans.* **2016**, *45*, 98–106. [[CrossRef](#)] [[PubMed](#)]
19. Baniodeh, A.; Anson, C.E.; Powell, A.K. Ringing the changes in  $\text{Fe}^{\text{III}}/\text{Yb}^{\text{III}}$  cyclic coordination clusters. *Chem. Sci.* **2013**, *4*, 4354–4361. [[CrossRef](#)]
20. Schmidt, S.; Prodius, D.; Novitchi, G.; Mereacre, V.; Kostakis, G.E.; Powell, A.K. Ferromagnetic heteronuclear  $\{\text{Fe}_4(\text{Er},\text{Lu})_2\}$  cyclic coordination clusters based on ferric wheels. *Chem. Commun.* **2012**, *48*, 9825–9827. [[CrossRef](#)] [[PubMed](#)]
21. Mezei, G.; Zaleski, C.M.; Pecoraro, V.L. Structural and Functional Evolution of Metallacrowns. *Chem. Rev.* **2007**, *107*, 4933–5003. [[CrossRef](#)] [[PubMed](#)]
22. Ostrowska, M.; Fritsky, I.O.; Gumienna-Kontecka, E.; Pavlishchuk, A.V. Metallacrown-based compounds: Applications in catalysis, luminescence, molecular magnetism, and adsorption. *Coord. Chem. Rev.* **2016**, *327*, 304–332. [[CrossRef](#)]
23. Pecoraro, V.L. Structural characterization of  $[\text{VO}(\text{salicylhydroximate})(\text{CH}_3\text{OH})]_3$ : Applications to the biological chemistry of vanadium(V). *Inorg. Chim. Acta.* **1989**, *155*, 171–173. [[CrossRef](#)]
24. Chow, C.Y.; Guillot, R.; Rivière, E.; Kampf, J.W.; Mallah, T.; Pecoraro, V.L. Synthesis and Magnetic Characterization of Fe(III)-Based 9-Metallacrown-3 Complexes Which Exhibit Magnetorefrigerant Properties. *Inorg. Chem.* **2016**, *55*, 10238–10247. [[CrossRef](#)] [[PubMed](#)]
25. Flamourakis, A.G.; Kalofolias, D.A.; Siczek, M.; Lis, T.; Brechin, E.K.; Milios, C.J. New members of the  $[\text{Mn}_6/\text{oxime}]$  family and analogues with converging  $[\text{Mn}_3]$  planes. *J. Coord. Chem.* **2016**, *69*, 826–840. [[CrossRef](#)]
26. Kessissoglou, D.P.; Bodwi, J.J.; Kampf, J.; Samara, C.D.; Pecoraro, V.L. Pseudohalide complexation by manganese 12-metallacrowns-4 complexes. *Inorg. Chim. Acta* **2002**, *331*, 73–80. [[CrossRef](#)]
27. Seda, S.H.; Janczak, J.; Lisowski, J.I. Synthesis and reactivity of copper(II) metallacrowns with (S)-phenylalanine and 2-picolinedihydroxamic acids. *Inorg. Chim. Acta* **2006**, *359*, 1055–1063. [[CrossRef](#)]
28. Samara, C.D.; Alevizopoulou, L.; Iordanidis, L.; Samaras, E.; Kessissoglou, D.P. 15-MC-5 manganese metallacrowns hosting herbicide complexes. Structure and bioactivity. *J. Inorg. Biochem.* **2002**, *89*, 89–96. [[CrossRef](#)]
29. Kremlev, K.V.; Samsonov, M.A.; Zabrodina, G.S.; Arapova, A.V.; Yunin, P.A.; Tatarsky, D.A.; Plyusnin, P.E.; Katkova, M.A.; Ketkov, S.Y. Copper(II)–cerium(III) 15-metallacrown-5 based on glycinehydroxamic acid as a new precursor for heterobimetallic composite materials on carbon nanotubes. *Polyhedron* **2016**, *114*, 96–100. [[CrossRef](#)]
30. Meng, Y.X.; Yang, H.; Li, D.C.; Zeng, S.Y.; Chen, G.F.; Li, S.L.; Dou, J.M. Synthesis, crystal structure, DNA-binding and magnetism of copper 15-metallacrown-5 complexes based on glycinehydroxamic acid ligand. *RSC Adv.* **2016**, *6*, 47196–47202. [[CrossRef](#)]
31. Jankolovits, J.; Kampf, J.W.; Pecoraro, V.L. Solvent Dependent Assembly of Lanthanide Metallacrowns Using Building Blocks with Incompatible Symmetry Preferences. *Inorg. Chem.* **2014**, *53*, 7534–7546. [[CrossRef](#)] [[PubMed](#)]
32. Jin, C.Z.; Wu, S.X.; Jin, L.F.; Wu, L.M.; Zhang, J. Esterification of the ligand: Synthesis, characterization and crystal structure of a iron(III) 18-metallacrown-6 complex with methyl 4-(5'-chlorosalicylhydrazinocarbonyl) butyrate. *Inorg. Chim. Acta* **2012**, *383*, 20–25. [[CrossRef](#)]
33. Shu, T.P.; Wen, J.L.; Feng, H.M.; Lei, K.W.; Liang, H.Z. Synthesis, structural characterization and magnetic properties of a novel metallacrown  $[\text{Fe}_6(\text{amshz})_6(\text{C}_3\text{H}_7\text{NO})_6] \cdot 6\text{CH}_3\text{OH}$ . *Solid State Sci.* **2009**, *11*, 2180–2183. [[CrossRef](#)]
34. Yang, W.; Yang, H.; Zeng, S.Y.; Li, D.C.; Dou, J.M. Unprecedented family of heterometallic  $\text{Ln}^{\text{III}}$ [18-metallacrown-6] complexes: Syntheses, structures, and magnetic properties. *Dalton Trans.* **2017**, *46*, 13027–13034. [[CrossRef](#)] [[PubMed](#)]
35. Phonsri, W.; Martinez, V.; Davies, C.G.; Jameson, G.N.L.; Moubaraki, B.; Murray, K.S. Ligand effects in a heteroleptic bis-tridentate iron(III) spin crossover complex showing a very high  $T_{1/2}$  value. *Chem. Commun.* **2016**, *52*, 1443–1446. [[CrossRef](#)] [[PubMed](#)]

36. Zadrozny, J.M.; Graham, M.J.; Krzyaniak, M.D.; Wasielewski, M.R.; Freedman, D.E. Unexpected suppression of spin–lattice relaxation via high magnetic field in a high-spin iron(III) complex. *Chem. Commun.* **2016**, *52*, 10175–10178. [[CrossRef](#)] [[PubMed](#)]
37. Phonsri, W.; Harding, P.; Liu, L.; Telfer, S.G.; Murray, K.S.; Moubaraki, B.; Ross, T.M.; Jameson, G.N.L.; Harding, D.J. Solvent modified spin crossover in an iron(III) complex: Phase changes and an exceptionally wide hysteresis. *Chem. Sci.* **2017**, *8*, 3949–3959. [[CrossRef](#)] [[PubMed](#)]
38. Thorarinsdottir, A.E.; Gaudette, A.I.; Harris, T.D. Spin-crossover and high-spin iron(II) complexes as chemical shift  $^{19}\text{F}$  magnetic resonance thermometers. *Chem. Sci.* **2017**, *8*, 2448–2456. [[CrossRef](#)] [[PubMed](#)]
39. Sheldrick, G.M. A short history of SHELX. *Acta Crystallogr. Sect. A Fundam. Crystallogr.* **2008**, *64*, 112–122. [[CrossRef](#)] [[PubMed](#)]
40. Yamashita, T.; Hayes, P. Analysis of XPS Spectra of  $\text{Fe}^{2+}$  and  $\text{Fe}^{3+}$  Ions in Oxide Materials. *Appl. Surf. Sci.* **2008**, *254*, 2441–2449. [[CrossRef](#)]
41. Nouredine, M.; Salem, S.; Slim, E.; Tadeusz, L.; Houcine, N. Experimental and DFT characterization of the organic–inorganic monohydrated Co(II) complex with 2,6-diaminopyridine ligand,  $(\text{C}_5\text{H}_8\text{N}_3)_2[\text{CoBr}_4]\cdot\text{H}_2\text{O}$ . *J. Mol. Struct.* **2016**, *1105*, 16–24. [[CrossRef](#)]
42. Jin, Z.M.; Pan, Y.J.; Xu, D.J.; Xu, Y.Z. The 1:1 complex of 4-nitrophenol and 4-methylpyridine. *Acta Cryst.* **2000**, *56*, 69–70. [[CrossRef](#)]
43. Haddad, S.F.; Al-Far, R.H. 2,6-Diaminopyridinium bromide monohydrate. *Acta Cryst.* **2003**, *59*, 1444–1446. [[CrossRef](#)]
44. Chow, C.Y.; Eliseeva, S.V.; Trivedi, E.R.; Nguyen, T.N.; Kampf, J.W.; Petoud, S.; Pecoraro, V.L.  $\text{Ga}^{3+}/\text{Ln}^{3+}$  Metallacrowns: A Promising Family of Highly Luminescent Lanthanide Complexes That Covers Visible and Near-Infrared Domains. *J. Am. Chem. Soc.* **2016**, *138*, 5100–5109. [[CrossRef](#)] [[PubMed](#)]
45. Azar, M.R.; Boron, T.T.; Lutter, J.C.; Daly, C.I.; Zegalia, K.A.; Nimthong, R.; Ferrence, G.M.; Zeller, M.; Kampf, J.W.; Pecoraro, V.L.; et al. Controllable Formation of Heterotrimetallic Coordination Compounds: Systematically Incorporating Lanthanide and Alkali Metal Ions into the Manganese 12-Metallacrown-4 Framework. *Inorg. Chem.* **2014**, *53*, 1729–1742. [[CrossRef](#)] [[PubMed](#)]
46. Wan, Y.H.; Zhang, L.P.; Jin, L.P.; Gao, S.; Lu, S.Z. High-Dimensional Architectures from the Self-Assembly of Lanthanide Ions with Benzenedicarboxylates and 1,10-Phenanthroline. *Inorg. Chem.* **2003**, *42*, 4985–4994. [[CrossRef](#)] [[PubMed](#)]
47. Lin, S.Y.; Xu, G.F.; Zhao, L.; Guo, Y.N.; Guo, Y.; Tang, J. Observation of slow magnetic relaxation in triple-stranded lanthanide helicates. *Dalton Trans.* **2011**, *40*, 8213–8217. [[CrossRef](#)] [[PubMed](#)]



© 2018 by the authors. Licensee MDPI, Basel, Switzerland. This article is an open access article distributed under the terms and conditions of the Creative Commons Attribution (CC BY) license (<http://creativecommons.org/licenses/by/4.0/>).